Emulation of anamorphic imaging on the SHARP EUV mask microscope

Markus P. Benk*, Antoine Wojdyla, Weilun Chao, Farhad Salmassi, Sharon Oh, Yow-Gwo Wang, Ryan H. Miyakawa, Patrick P. Naulleau, Kenneth A. Goldberg
Center for X-ray Optics, Lawrence Berkeley National Laboratory,
1 Cyclotron Road, Berkeley, CA 94720

ABSTRACT

The SHARP High numerical aperture Actinic Reticle review Project is a synchrotron-based, extreme ultraviolet (EUV) microscope dedicated to photomask research. SHARP emulates the illumination and imaging conditions of current EUV lithography scanners and several generations into the future. An anamorphic imaging optic with increased mask side-NA in the horizontal and increased demagnification in the vertical direction has been proposed to overcome limitations of current multilayer coatings and extend EUV lithography beyond 0.33 NA.[1] Zoneplate lenses with an anamorphic 4x/8x NA of 0.55 are fabricated and installed in the SHARP microscope to emulate anamorphic imaging. SHARP's Fourier synthesis illuminator with a range of angles exceeding the collected solid angle of the newly designed elliptical zoneplates can produce arbitrary angular source spectra, matched to anamorphic imaging. A target with anamorphic dense features down to 50-nm critical dimension is fabricated using 40-nm of nickel as the absorber. In a demonstration experiment anamorphic imaging at 0.55 4x/8xNA and 6º central ray angle is compared to conventional imaging at 0.5 4xNA and 8º central ray angle. A significant contrast loss in horizontal features is observed in the conventional images. The anamorphic images show the same image quality in the horizontal and vertical directions.

Keywords: EUV, anamorphic, mask, microscope, zone plate, High-NA

1. INTRODUCTION

The insertion of extreme ultraviolet lithography (EUVL) into production is likely to happen at the 7-nm logic node, corresponding to k_1 factors well below 0.5 at 0.33 numerical aperture (NA).[2] Feature sizes at these nodes require the use of resolution enhancement techniques in EUVL from the start, not leaving much room to further decrease critical dimensions (CD) without using double patterning.[3] The next generation of EUVL at higher NA is under development now and will be required soon after the insertion of EUVL into production in order to keep the technology on track down to smaller feature sizes.

The wafer-side NA of a lithography system may be increased by either increasing the mask-side NA, increasing the demagnification of the system, or a combination of the two. An increased mask-side NA creates an increased angular extent of the incoming and outgoing light cones. Separating the cones requires an increased central ray angle (CRA) at the photomask to avoid overlap. In the plane of incidence the increased range of angles on the photomask, offset by an increased CRA, exceeds the angular bandwidth of current multilayer reflective coatings, thus reducing image contrast. Perpendicular to the plane of incidence, the range of angles does not exceed the bandwidth of the multilayer coating. For horizontal features, perpendicular to the plane of incidence, the illumination is offset by the central ray angle, and shadowing from the thick absorber can degrade imaging performance. For vertical features, parallel to the plane of incidence, the illumination is centered, causing less shadowing.

*mpbenk@lbl.gov; phone 1 510 486-5680; fax 1 510 486-4550; sharp.lbl.gov

Extreme Ultraviolet (EUV) Lithography VII, edited by Eric M. Panning, Proc. of SPIE Vol. 9776, 97761J · © 2015 SPIE · CCC code: 0277-786X/15/$18 · doi: 10.1117/12.2219294

EUV projection lenses at higher demagnification ratios, beyond 4x show acceptable imaging performance. But printing one full field at two-times higher demagnification either requires a photomask with four times the surface area, or the field needs to be stitched from four quarter-field exposures. Both of these options are considered economically not viable[1].

Zeiss and ASML have proposed an anamorphic projection optic with increased mask side NA perpendicular to the plane of incidence and increased demagnification in the plane of incidence.[4] Such a design avoids high angles of incidence on the photomask in the plane of incidence (that would degrade image quality) while preserving the demagnification perpendicular to the plane of incidence. This allows stitching one full field on the wafer from two half-field exposures instead of four quarter-fields. The angular bandwidth of the multilayer is used most efficiently. An anamorphic projection optic with a wafer-side NA of 0.55 is discussed in Ref 5.

Aerial mask imaging tools are currently used in EUV research and process development and will be required for EUV production. SHARP is a synchrotron-based, actinic, EUV mask microscope, located at a bending-magnet beamline at the Advanced Light Source at Lawrence Berkeley National Laboratory. Since its commissioning in 2013, SHARP has contributed to many aspects of EUV mask technology, including defects,[6] their detection[7] and printability,[8] repairs,[8] substrate roughness,[9] impact of non-telecentricity[10] or multilayer properties.[11] For an overview of SHARP, see Ref 12.

SHARP is designed to emulate imaging in EUV scanners. The tool records a series of aerial images of a feature or defect on the photomask, matching the mask-side NA of the scanner and emulating the angular spectrum of the illumination, including the chief-ray angle and azimuthal rotation of the plane of incidence across the field. The SHARP aerial image therefore is similar to the wafer print, thus allowing the user to assess the characteristics of a feature or defect with respect to printing on a wafer. Figure 1 shows a comparison of a mask-SEM (Scanning Electron Microscopic image) (a), SHARP aerial image (b), and wafer-SEM (c). The images are taken from Ref 13. The SHARP aerial image closely matches the wafer print. The mask-SEM shows the defect but does not reveal the extent of the damage to the multilayer surrounding the visible defect.

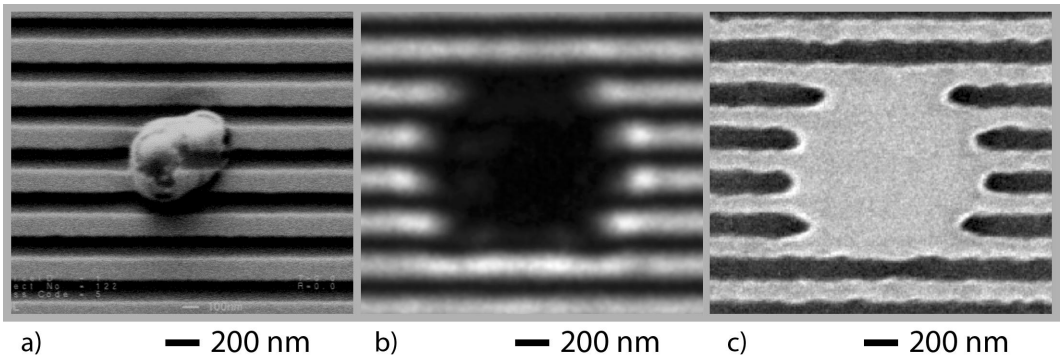

Figure 1. Visual comparison of a large defect,[13] imaged with (a) mask-SEM, (b)SHARP EUV mask microscope and (c) wafer-SEM.

SHARP uses a wide range off-axis Fresnel zoneplate lenses as imaging optics, matching the mask-side NA of current and future generations of EUVL, including the ASML ADT and NXE 3100 to 3500 scanners. The tool's standard zoneplates range from 0.25 4xNA up to 0.625 4xNA. A resolution of 22 nm half pitch (hp) on the mask side, corresponding to 5.5 nm hp on the wafer side in a 4x lithography system, has been demonstrated for the 0.625 4xNA lens.[14] To emulate the source angular spectrum of the scanner, SHARP has a fully programmable Fourier synthesis illuminator.[15]

SHARP's flexible design allows it to respond to new developments in EUVL and to emulate arbitrary technologies under consideration, to enable research many years into the future of EUV lithography. Recently, SHARP has been upgraded to emulate anamorphic imaging, providing a platform for research in this emerging area.

2. EMULATION OF ANAMORPHIC IMAGING

SHARP emulates the source angular spectrum and mask-side NA values; emulating anamorphic imaging requires the corresponding illuminator and elliptical mask-side illumination solid angle. Since SHARP's Fourier synthesis illuminator can reach angles of incidence up to 19° off-axis at the mask (well beyond typical multilayer angular bandpass limits), all anamorphic imaging configurations can be generated. Figure 2 shows a pixelated cross pole illuminator, rendered for the 0.33 4xNA lens at 6º CRA (a), 0.5 4xNA lens at 8º CRA (b) and for anamorphic imaging at 0.55 4x/8xNA and 6º CRA (c), in comparison. The images are recorded with a YAG scintillator camera, installed in the tool for monitoring the source angular spectrum. The individual pupil channels (pixels) can be seen in the high-NA pupils. For 0.33 4xNA the angular divergence of the synchrotron beam matches the solid angle of the pupil channels, making them indistinguishable.

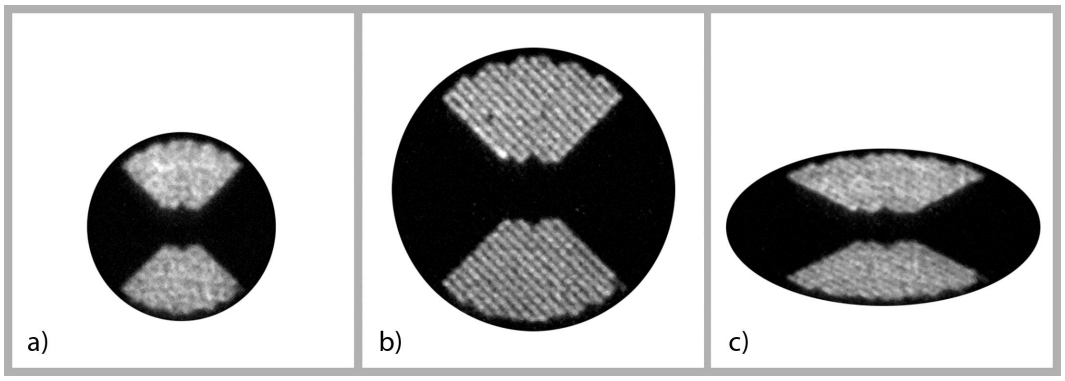

Figure 2. Pixelated cross pole illuminator, matched to (a) the 0.33 4xNA lens at 6º CRA, (b) 0.5 4xNA lens at 8º CRA and to (c) anamorphic imaging at 0.55 4x/8xNA and 6º CRA in comparison, recorded with a YAG scintillator camera in SHARP microscope.

2.1 Zoneplate

Figure 3 shows the apertures (gray) of a 0.33 4xNA zoneplate at 6º CRA, a 0.5 4xNA zoneplate at 8º CRA and a 0.55 4x/8xNA zoneplate for anamorphic imaging at 6º CRA in comparison. The difference in the angular range with respect to the normal ray on the photomask can been seen. Figure 4 shows the calculated reflectivity of a typical Mo/Si multilayer on a photomask at 13.5-nm wavelength as a function of the angle of incidence. The reflectivity curve is almost flat from normal incidence to about 11º from normal, and then starts rolling off towards larger angles. The end of the useable angular bandwidth at 11º is marked in Figures 3 and 4.

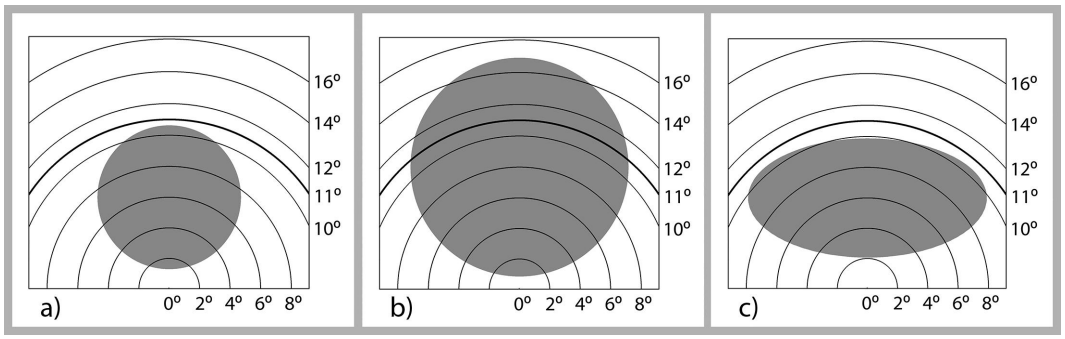

Figure 3. Apertures of (a) a 0.33 4xNA zoneplate at 6º CRA, (b) 0.5 4xNA zoneplate at 8º CRA and (c) 0.55 4x/8xNA zoneplate for anamorphic imaging at 6º CRA in comparison and range of angles of the associated ray cones.

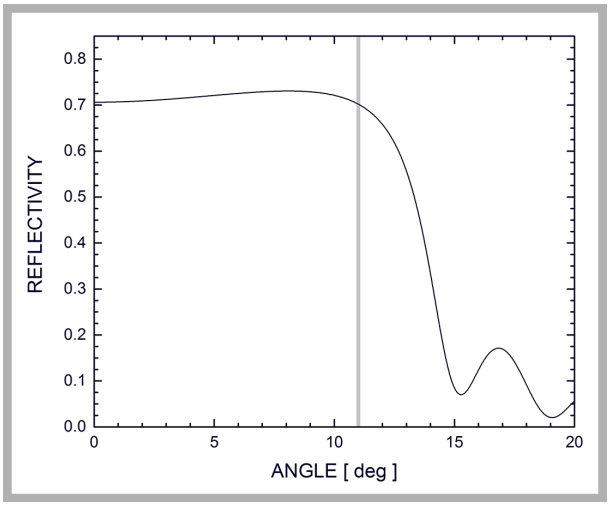

Figure 4. Calculated reflectivity of a typical multilayer coating on an EUV photomask at 13.5-nm wavelength as a function of the angle of incidence.

The aperture of a zoneplate for anamorphic imaging is defined by the intersection of the elliptic cone of a given NA with a plane, tilted by the CRA (6º). The normal distance from the tip of the cone to the intersecting plane sets the working distance of the zoneplate. The mask-side coherent resolution of the lens $r_c = 0.5\lambda / NA$ is 54-nm hp in the lateral, high-NA (4x) orientation, which is the *x*-direction in the image, and is 108-nm in the low-NA (8x) orientation, which is the *y*-direction in the image. The zoneplate, as a single optical element does not provide anamorphic imaging, i.e., different magnifications in *x* and *y*. Collecting the proper solid angle however captures the characteristics of the anamorphic image and the aspect ratio can easily be corrected, scaling the digital image in one dimension.

The 0.55 4x/8x NA zoneplate is fabricated in three different working distances: 360 µm, 320 µm and 275 µm with approximate magnifications of 1250x, 1400x, and 1640x. The lowest magnification corresponds to 5 pixels per resolution element in the high-NA (4x) orientation. In the low-NA (8x) orientation there are twice as many pixels per resolution element in the raw image. After scaling the image by a factor two, the number of pixels per resolution element matches in *x* and *y* consequently. The lowest-magnification lens produces the brightest picture and offers the largest working distance. For experiments, where higher sampling is desired, the highest magnification with 6.5 pixels per resolution element can be used.

Like SHARP's standard zoneplates, the 0.55 4x/8xNA zoneplates are patterned with e-beam lithography and electroplated using 35 nm of gold on a 100-nm silicon nitride membrane. The SEM-images in Figure 5 show one of the anamorphic zoneplates (a) and a detail of its outer zones (b). The zone pattern is not resolved in Figure 5 (a), causing a Moiré pattern.

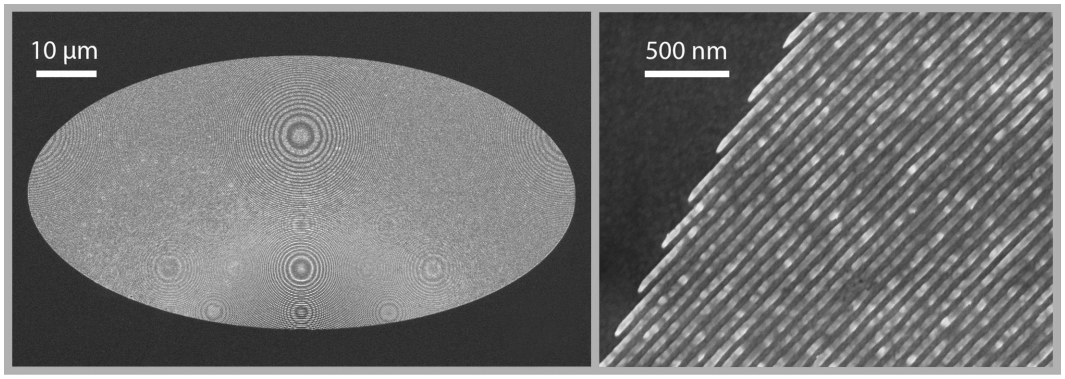

Figure 5. SEM-image of (a) a zoneplate lens with an anamorphic aperture and (b) detail image, showing the outer zones.

2.2 Target fabrication

In order to demonstrate anamorphic imaging on the SHARP microscope, a set of anamorphic test patterns is fabricated. Three different aspect ratios of the patterns are realized: 4x/8x for the anamorphic imaging demonstration; standard 4x, as a reference; and 4.8x/7.5x. This latter aspect ratio is discussed in Ref 5. Just like 4x/8x it allows for stitching one full-field from two half-fields, using a slightly wider and less tall region of the photomask and collecting a slightly different solid angle from the mask. Zoneplates for this aspect ratio will be included in the next production run.

Aiming at a short production time, the target is patterned in-house at the CXRO Nanofabrication laboratory, on a silicon wafer in a nickel lift-off process instead of using an EUV photomask blank with a tantalum-based absorber. The wafer is coated with a standard Mo/Si multilayer and ruthenium capping layer. The wafer is then coated with PMMA and patterned using electron beam lithography. After development, a 2-nm assist layer of chrome is deposited for adhesion, and 40 nm of nickel are deposited as the absorber. Chrome and nickel adhere to the clear multilayer. The chrome and nickel on the resist are lifted-off together with the resist material in an etch-step, leaving nickel patterns. The wafer is then mounted on a mask substrate for loading into SHARP. The target has patterns down to 50-nm CD. Figure 6 shows three images of the LBNL logo that is part of the test patterns. The conventional 4x (a), 4x/8 (b) and 4.8/7.5x aspect ratios (c) are shown side-by-side. The images are recorded in the SHARP microscope at a 4xNA of 0.33.

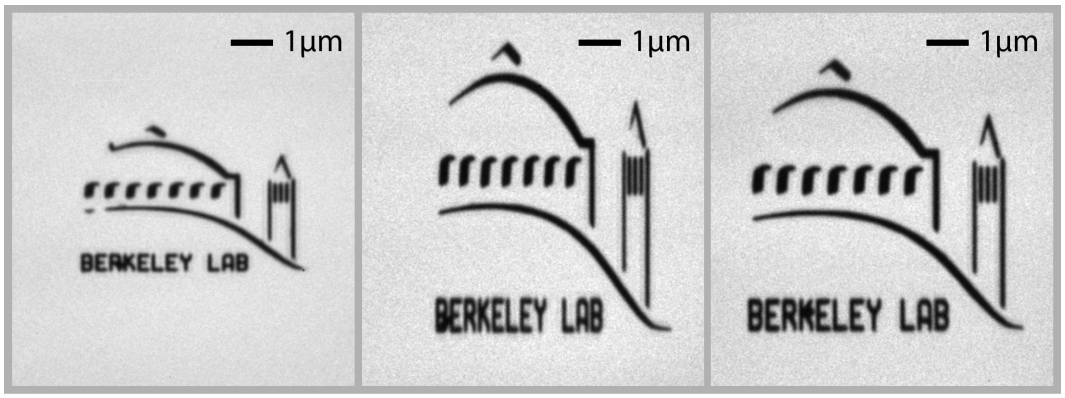

Figure 6. SHARP aerial images of (a) 4x reference pattern, and (b) anamorphic 4x/8x and (c) 7.5x/4.8x test patterns.

3. IMAGING RESULTS

Different test patterns are imaged using Quasar-45 illumination with 45º arc angle and an inner σ of 0.2 and outer σ of 0.9. The parameter σ, ranging from zero to one, describes the angular extend of the illumination relative to the NA of the imaging optic. Figure 7 (a) shows a SHARP image of a test pattern with 50-nm cd (mask scale), recorded with the 0.55 4x/8xNA lens. Figure 7 (b) shows the same image, scaled to match the difference in magnification in *x* and *y* in the anamorphic image. Scaling of the image is shown here in an example. Further anamorphic images, shown in this paper, are already scaled and interpolated to a finer grid.

Images of a test pattern with 50-nm cd (mask scale) are shown in Figure 8, comparing anamorphic imaging at 0.55 4x/8xNA (6º CRA) (a) to conventional (isomorphic) imaging at 0.5 4xNA (8º CRA) (b). In the anamorphic image, the pattern is resolved, showing the same image quality on horizontal and vertical features. In the conventional image, vertical features are resolved but the image contrast is reduced on horizontal features. This is due to the angular range of the collected solid angle exceeding the angular bandwidth of the multilayer and due to vertical shadowing from resist features, as discussed in the introduction.

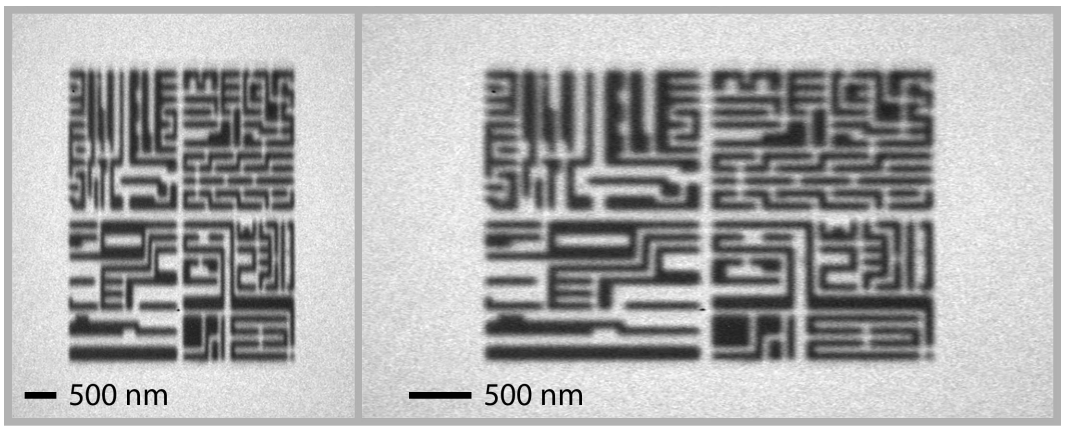

Figure 7. (a) SHARP image of anamorphic test pattern with 50-nm cd (mask scale) and (b) scaled version of the image with corrected magnifications in *x* and *y*.

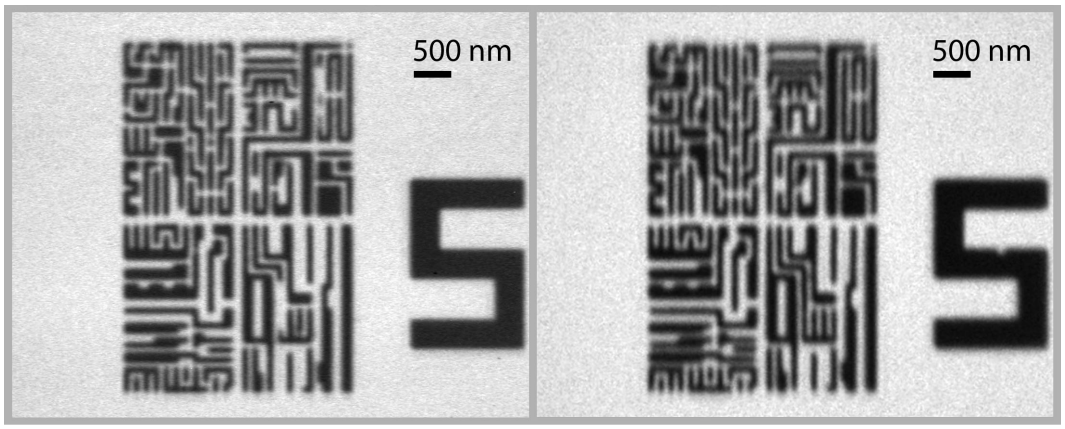

Figure 8. SHARP aerial images of a test pattern with 50-nm cd (mask scale), comparing (a) anamorphic imaging at 0.55 4x/8xNA (6º CRA) to (b) conventional (isomorphic) imaging at 0.5 4xNA (8º CRA).

50-nm cd elbows (mask scale) are shown in Figure 9, again comparing anamorphic imaging at 0.55 4x/8xNA (6º CRA) (a) to conventional (isomorphic) imaging at 0.5 4xNA (8º CRA) (b). As in the previous example, the anamorphic image shows the same image quality in *x* and *y*. In the conventional image only vertical features are resolved. The high angles of incidence and shadowing from the absorber lead to loss of contrast on horizontal features. Figure 9 (c) shows an SEM image of the 4x elbow on the target. The SEM shows some small pattern defects that can be seen in the SHARP image as well. The pattern quality on the mask is equal in the horizontal and vertical directions, thus the imaging non-uniformity seen in SHARP is wholly attributable to image formation at wavelength.

Cross section plots through the horizontal and vertical features in the elbows from Figure 9 are shown in Figure 10. The cross sections are averaged over 30 pixels, parallel to the line directions. The profiles are normalized by setting the intensity of the clear region around the elbow to be one. The horizontal and vertical line profiles from the anamorphic image (a) are similar, with a modulation of 44%. The cross section plot of the vertical features in the conventional image (b) shows 52% modulation (higher than the modulation in the anamorphic image), while the modulation on horizontal features is only 19%. A higher average intensity in the lines and spaces, found in the anamorphic image indicates a higher background level. More scattered light from the bright-field target reaching the CCD at the lower angular separation (6º CRA) in the anamorphic image is a possible source of increased background and consequently decreased modulation, compared to the vertical lines in the conventional image at 8º CRA. An increased background is also found in the large absorber feature (the number five) in the anamorphic image from Figure 8.

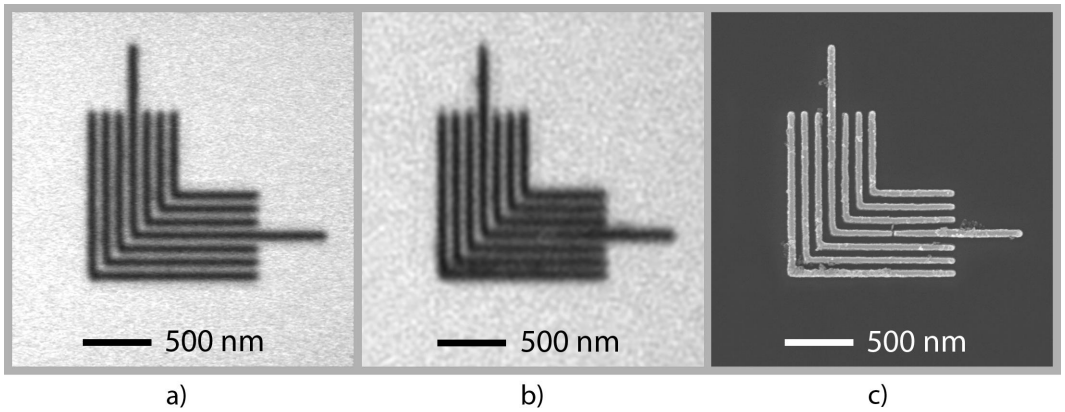

Figure 9. SHARP aerial images of 50-nm cd elbows (mask scale), comparing (a) anamorphic imaging at 0.55 4x/8xNA (6º CRA) to (b) conventional imaging at 0.5 4xNA (8º CRA), and (c) SEM-image of the 4x elbow on the target (c).

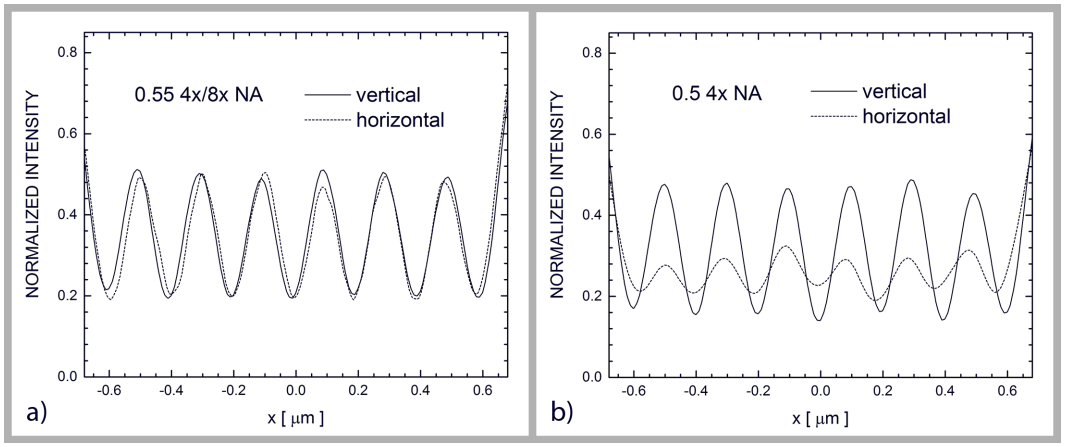

Figure 10. Cross section of the horizontal and vertical features of the 50-nm cd elbows from Fig 9, comparing (a) anamorphic imaging at 0.55 4x/8xNA (6º CRA) to (b) conventional imaging at 0.5 4xNA (8º CRA).

The SHARP images, shown in Figure 9, are taken from through-focus series, recorded by varying the object distance in 300-nm steps. Figure 11 shows plots of the modulation in the elbows through-focus, comparing (a) anamorphic and (b) conventional imaging. The evolution of the images through-focus is shown in Figure 12. Aside from the overall lower modulation on horizontal features, the conventional series shows the same through-focus characteristics in *x* and *y*. On vertical features the modulation through-focus in the anamorphic data compares well to the characteristics of the conventional series. For horizontal features, the modulation curve of the anamorphic data is almost flat within a range of 2.4 μm, The depth of field exceeds the focal range covered in the series. Considering the factor 2 between the horizontal and vertical NA of the anamorphic lens, the depth of field (on the mask-side) is expected to be four times larger for horizontal features. In EUV scanners the depth of focus (on the wafer-side) is the primary concern. It is smaller than the depth of field by a ratio of the demagnification squared (i.e. a factor of 16 for a 4x system). Since the exit pupil is circular, depth of focus is expected to be uniform in an anamorphic scanner.

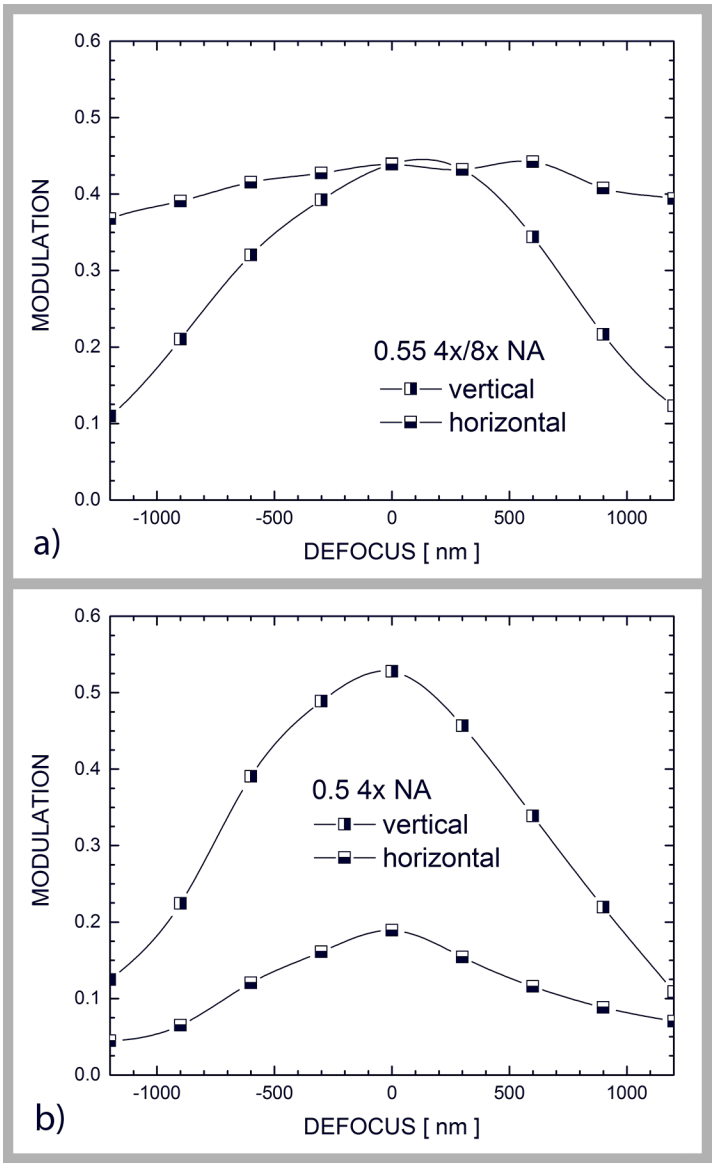

Figure 11. Modulation of horizontal and vertical features through-focus in the (a) anamorphic and (b) conventional series of SHARP images, shown in Fig 12.

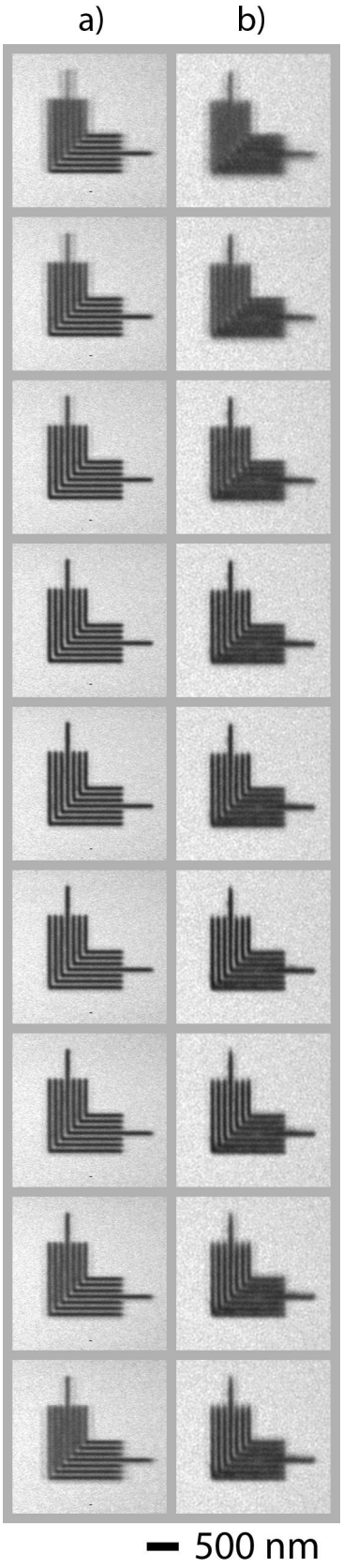

Figure 12. Through-focus series of SHARP images, comparing through-focus behavior in (a) anamorphic imaging at 0.55 4x/8xNA (6º CRA) to (b) conventional imaging at 0.5 4xNA (8º CRA).

4. SUMMARY

SHARP is an actinic EUV mask-imaging microscope targeted at a wide range of applications in EUV photomask research and development. The tool is designed to emulate imaging in EUV lithography scanners. The generation of EUVL succeeding the 0.33 NA systems will likely employ anamorphic imaging with different horizontal and vertical demagnification. SHARP is upgraded to emulate scanners with anamorphic projection optics.

Zoneplate lenses with an anamorphic 4x/8x NA of 0.55 are fabricated and installed in the tool. SHARP's Fourier synthesis illuminator readily produces source angular spectra matched to anamorphic imaging. Anamorphic test patterns down to 50-nm cd dense features are written on a multilayer-coated silicon wafer using 40 nm of nickel as the absorber material.

Test patterns are imaged in a demonstration experiment, comparing anamorphic imaging at 0.55 4x/8x NA and 6º CRA to conventional imaging at 0.5 4xNA and 8º CRA. While the anamorphic images show the same image quality in the horizontal and vertical directions, conventional imaging suffers from a significant horizontal feature contrast loss which can be attributed to the limited angular bandwidth of the multilayer coating and shadowing from absorber features. The mask-side through-focus behavior of anamorphic and conventional EUV-imaging systems is discussed.

The SHARP microscope provides a versatile platform for research related to anamorphic imaging in EUV lithography today. The consideration of various demagnifications and pupil aspect ratios, and illumination patterns can be used to guide progress in this area without extensive modifications to all-reflective actinic mask-imaging microscopes.

REFERENCES

[1] Van Schoot, J., van Ingen Schenau, K., Valentin, C., Migura, S., "EUV lithography scanner for sub 8 nm resolution," *Proc. SPIE* 9422, 94221F (2015).

[2] Burkhardt, M., Raghunathan, A., "Best Focus Shift Mechanism for Thick Masks," *Proc. SPIE* 9422, 94220X (2015).

[3] Civay, D. E., Hosler, E. R., Cantone, J. R., Thiruvengadam, S., Schroeder, P., "EUV and optical lithographic pattern shift at the 5nm node," SPIE 9776 Extreme Ultraviolet (EUV) Lithography VII, book of abstracts, 9776-43 (2016).

[4] Kneer B., Migura, S., Kaiser, W., Neumann, J. T., van Schoot, J., "EUV Lithography Optics for sub 9 nm Resolution," *Proc. SPIE* 9422, 94221G (2015).

[5] Heil T., Kneer, B., Migura, S., Ruoff, J., Rösch, M., Neumann, J. T., Kaiser, W., van Schoot, J., "Anamorphic High NA Optics enabling EUV Lithography with sub 8nm Resolution," 2015 International Symposium of Extreme Ultra Violet Lithography, Oct. 7, 2015.

[6] Gallagher, E., Wagner, A., Lawliss, M., McIntyre, G., Seki, K., Isogawa, T., Nash, S., "Learning from native defects on EUV mask blanks," *Proc. SPIE* 9256, 92560K (2014).

[7] Wang, Y.-G., Miyakawa, R., Chao, W., Benk, M., Wojdyla, A., Donoghue, A., Johnson, D., Goldberg, K., Neureuther, A., Liang, T., Naulleau, P., "Enhancing defect detection with Zernike phase contrast in EUV multilayer blank inspection." *Proc. SPIE* 9422, 94221C (2015).

[8] Lawliss, M., Gallagher, E., Hibbs, M., Seki, K., Isogawa, T., Robinson, T., LeClaire, J., "Repairing native defects on EUV mask blanks," *Proc. SPIE* 9235, 923516 (2014).

[9] Yan, P.-Y., Zhang, G., Gullikson, E., Goldberg, K. A., Benk, M. P., "Understanding EUV mask blank surface roughness induced LWR and associated roughness requirement," *Proc. SPIE* 9422, 94220J (2015).

[10] Raghunathan, S., Wood II, O. R., Mangat, P., Verduijn, E., Philipsen, V., Hendrickx, E., Jonckheere, R., Goldberg, K. A., Benk, M. P., Kearney, P., Levinson, Z., Smith, B. W., "Experimental measurements of telecentricity errors in high-numerical-aperture extreme ultraviolet mask images," *J. Vac. Sci. Technol. B* 32, 06F801 (2014).

[11] Philipsen, V., Hendrickx, E., Verduijn, E., Raghunathan, S., Wood, O., Soltwisch, V., Scholze, F., Davydova, N., Mangat, P., "Imaging impact of multilayer tuning in EUV masks, experimental validation," *Proc. SPIE* 9235, 92350J (2014).

[12] Goldberg, K. A., Benk, M. P., Wojdyla, A., Mochi, I., Rekawa, S. B., Allezy, A. P., Dickinson, M. R., Cork, C. W., Chao, W., Zehm, D. J., Macdougall, J. B., Naulleau, P. P., Rudack, A., "Actinic mask imaging: recent results and future directions from the SHARP EUV microscope," *Proc. SPIE* 9048, 90480Y (2014).
[13] Goldberg, K. A., Benk, M. P., Wojdyla, A., Verduijn, E., Wood II, O. R, Mangat, P., "EUV actinic brightfield mask microscopy for predicting printed defect images," *Proc. of SPIE* 9635, 963514 (2015).
[14] Benk, M. P., Goldberg, Wojdyla, A., Anderson, C. N., Salmassi, F., Naulleau, P. P., Kocsis, M., "Demonstration of 22-nm half pitch resolution on the SHARP EUV microscope," J. Vac. Sci. Technol. B 33, F06FE01 (2015).
[15] Naulleau, P. P., Goldberg, K. A., Batson, P., Bokor, J., Denham, P., Rekawa, S., "Fourier-synthesis custom-coherence illuminator for extreme ultraviolet microfield lithography," *Appl. Opt.* 42 (5), 820-826 (2003).